Journal of the European Ceramic Society 19 (1999) 2125–2131

PII: S0955-2219(99)00026-6
0955-2219/99/$ - see front matter

Fabrication and Microstructure of Al_2O_3–ZrO_2(3Y)–SiC Nanocomposites

H. Z. Wang*, L. Gao and J. K. Guo

The State Key Lab on High Performance Ceramics and Superfine Microstructure, Shanghai Institute of Ceramics, Chinese Academy of Sciences, Shanghai 200050, People's Republic of China

(Received 15 August 1998; accepted 12 January 1999)

Abstract

Al_2O_3–ZrO_2(3Y)–SiC composite powder was prepared by the heterogeneous precipitation method. Calcinating temperature of the powder was important to obtain dense sintered body. The nanocomposites were got by hot-pressing, and addition of ZrO_2 did not raise the sintering temperature. Some Al_2O_3 grain shape was elongated, and Al_2O_3 grain size was about μm. Nano SiC particles were observed uniformly distributing throughout the composites, and most of them were located within the matrix grains. Because SiC particles located within ZrO_2 grains influenced the phase transformation of ZrO_2, the sintering of nanocomposites, which controlled grain size and transformable ZrO_2 amount, become important to get high performance. The strength of 80 wt% Al_2O_3–15 wt% ZrO_2–5 wt% SiC nanocomposites was 555 MPa, and toughness was 3·8 MPa $m^{1/2}$, which were higher than those of monolithic Al_2O_3 ceramics. © *1999 Elsevier Science Limited. All rights reserved*

Keywords: composites, microstructure-final, mechanical properties, Al_2O_3, SiC, D. ZrO_2.

1 Introduction

Al_2O_3 ceramics are essential structural materials, but low mechanical properties limit their applications. Since Niihara reported that composites reinforced with submicrometer or nanoscale second phase called nanocomposites have excellent mechanical properties,[1,2] Al_2O_3-SiC nanocomposites have become an interested material to overcome the inherent demerit of Al_2O_3 ceramics.[3] According to Niihara's investigation, addition of 5 vol% SiC particles whose size was about 0·3 μm could increase the strength of hot-pressed alumina from 350 MPa to over 1 GPa and the fracture toughness from 3·2 to 4·7 MPa $m^{1/2}$, and further annealing enhanced the strength of this nanocomposite to 1·5 GPa. It can be seen that the strength improvement of Al_2O_3–SiC nanocomposites was distinct, but toughness only increases a little compared with monolithic Al_2O_3 ceramics. Since Niihara's pioneer work, many researchers have intensively studied the processing and microstructure of Al_2O_3–SiC nanocomposites,[4–6] and found the details of processing were very important to get high performance, but considerable improvement of toughness has not been observed yet, compared with monolithic Al_2O_3.

In Al_2O_3–SiC nanocomposites the increase of mechanical properties could be attributed to residual stress fields, and other toughening mechanisms such as microcracking, crack tip shielding, crack branching, and crack deflection.[3] To enhance the toughness, more energy absorbed mechanisms are needed besides those listed above. Stress induced transformation of ZrO_2 is believed to be an effective toughening approach to Al_2O_3 ceramics,[7–9] and the toughness of ZrO_2 toughened Al_2O_3 ceramic (ZTA) is significantly higher than that of pure Al_2O_3. If stress induced transformation toughening can combine with other toughening mechanisms in nanocomposites, adding ZrO_2 to Al_2O_3–SiC system is hopeful to improve the toughness of nanocomposites. There are still few reports about Al_2O_3–ZrO_2–SiC nanocomposites, and the effect of ZrO_2 on Al_2O_3–SiC nanocomposites is uncertain. Therefore, it is interesting to study processing, microstructure, and properties of Al_2O_3–ZrO_2–SiC nanocomposites.

*To whom correspondence should be addressed. Fax: +86-021-62513903; e-mail: hzwang@kali.com.cn

2 Experimental

Al_2O_3–ZrO_2(3Y)–SiC composite powders were prepared by the heterogeneous precipitation method. The size of nanoscale SiC particles was about 70 nm (Beijing Institute of Chemical Metallurgy, CAS). The flow chart is shown in Fig. 1.

It is critical to disperse nanoscale SiC particles homogeneously into the matrix because SiC particles are fine and easy to aggregate. There are three ways to avoid their agglomerates: (1) ultrasonic vibrating to open agglomerates, (2) regulating pH to make the zeta potential high, (3) adding dispersants. Since some carbon remains may be left after adding dispersants, only the first two ways were adopted to produce good dispersion. The isoelectric point of SiC was determined to be between pH 3 and 5. If the pH value of SiC aqueous suspension is beyond this range, the charge of the particles is the same, and the SiC particles will repulse each other due to a static electric force, making it difficult to form agglomerates. For this reason, the pH value of the SiC aqueous suspension was regulated to 9–10 while constantly ultrasonic vibrating for 1 h. Then, $AlCl_3$, $ZrOCl_2$, $Y(NO_3)_3$ solution and ammonia were dripped into the SiC aqueous suspension simultaneously while the pH value was always maintained between 9 and 10, $Al(OH)_3$, $Zr(OH)_4$ and $Y(OH)_3$ precipitation including well-dispersed nano SiC particles were produced. After drying, calcining and wet-balling, Al_2O_3–ZrO_2(3Y)–SiC powder could be achieved. The nearly full density samples could be got by hot-pressing at temperatures between 1650 and 1700°C.

Sintered densities were measured using the Archimedes method. For mechanical testing, the hot pressed samples were cut and ground into rectangular bar specimens (4×3×30 mm). Fracture toughness was evaluated from the indentation fracture method,[10] and fracture strength was measured by the three point bending test. For the grain growth observation, samples were polished using diamond paste to a 1 μm finish, and thermally etched in nitrogen at temperatures between 1400 and 1600°C. The etched surface and the fracture cross section was examined using a scanning electron microscope (SEM), and the composite powder and other microstructure features of sintering bodies were examined using a transmission electron microscope (TEM). X-ray diffraction analyses were performed to determine the peak heights of tetragonal and monoclinic zirconia and the following equations were utilized to calculate the volume fraction of the monoclinic phase.[11]

$$V_m = \frac{pX_m}{1 + (p-1)X_m} \tag{1}$$

where X_m is the integrated intensity ratio and $P = 1{\cdot}340$

$$X_m = \frac{I_m(\bar{1}11) + I_m(111)}{I_m(\bar{1}11) + I_m(111) + I_t(101)}$$

Subscripts m and t represent the monoclinic and the tetragonal phases, respectively. I_m and I_t are the peak heights of these phases. V_m is the volume fraction of the monoclinic phase and that of the tetragonal phase is $V_t = 1 - V_m$

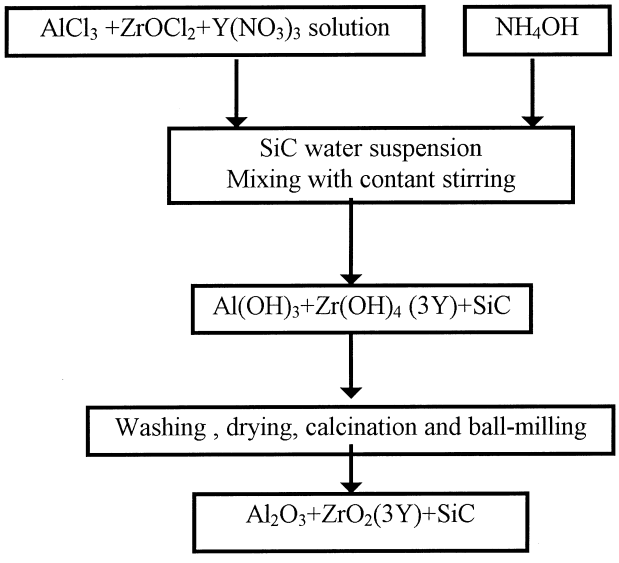

Fig. 1. Flow chart of the heterogeneous precipitation method.

3 Results and Discussion

3.1 The selection of the calcination temperature

During the preparation process of Al_2O_3–ZrO_2-SiC powder, the calcination temperature selection is important. Several phase transformations of Al_2O_3 and ZrO_2 would occur from room temperature to sintering temperature, which include γ-Al_2O_3 transforming to α-Al_2O_3 at 1200°C through several transition phases, and m-ZrO_2 changing to t-ZrO_2 at about 1000°C. Those transformations will cause the phase volume change, and influence sintering. In the procedure of ceramics, calcination is generally adopted to make phases stable and avoid the phase volume change. The high calcination temperature and long holding time is believed to be effective to raise phase stability. But high calcination temperature and long holding time will make powders lose their activities and form aggregate which will be unfavourable to sintering. The proper calcination temperature for powder is essential to obtain dense Al_2O_3–ZrO_2(3Y)–SiC nanocomposites with considerable properties.

After drying, the precipitate obtained from the heterogeneous precipitation was calcinated at different temperatures for 1 h, and examined by XRD. The phase transformations at different temperatures are shown in Fig. 2.

From Fig. 2, it can be seen that as-received precipitates included $Al(OH)_3$ and $Zr(OH)_4$, and their phases were bayerite (β-$Al_2O_3{\cdot}3H_2O$) and amorphous, respectively. After calcinating at 700°C bayerite disappeared, and peaks of oxide occurred. Peak intensity of t-ZrO_2, γ-Al_2O_3 (or other alumina transition phases) increased with the increment of calcination temperatures, and γ-Al_2O_3 transformed to α-Al_2O_3 completely above 1200°C. To select proper calcination temperature, the composite powders calcinated at 700 and 1100°C were hot-pressed and measured densities of sintering bodies respectively. It was found that integrated sintered bodies were difficult to obtain using the powder calcinated at 700°C. Although the heating rate was slowed, and the holding time was extended, the sintering samples still broke. From Fig. 2, it can be concluded that t-ZrO_2 in composite powder appeared but did not crystallize completely after calcinating at 700°C. t-ZrO_2 crystallization plus γ-Al_2O_3 transformation would produce high internal stress during the sintering of Al_2O_3–ZrO_2(3Y)–SiC nanocomposites, which could be beyond the endurance of bodies, and made sintering difficult. To avoid too much transformation during sintering, the composite powder was calcinated at 1100°C. This temperature (1100°C) was also the calcination temperature for most of ZrO_2 toughened Al_2O_3 ceramics (ZTA).[12,13] At this temperature, t-ZrO_2 crystallized completely, and Al_2O_3 was still the transition phase which made the composite powder processed relatively high activity. Piciacchio *et al.*[14] believed that the vermicular growth of α-Al_2O_3 into the transition alumina matrix during γ-Al_2O_3 phase transformation would result in relatively greater concentration of intragranular SiC, so the composite powder including γ-Al_2O_3 was expected to prepare intragranular nanocomposites. Dense sintering bodies could be obtained using the powder calcinated at 1100°C, which proved that 1100°C was the proper calcination temperature for Al_2O_3–ZrO_2(3Y)–SiC composite powder.

The specific surface area of Al_2O_3–ZrO_2(3Y)–SiC powder after calcinating at 1100°C was 13 m^2 g^{-1}, and morphology was shown in Fig. 3. The size of powder was about 100 nm.

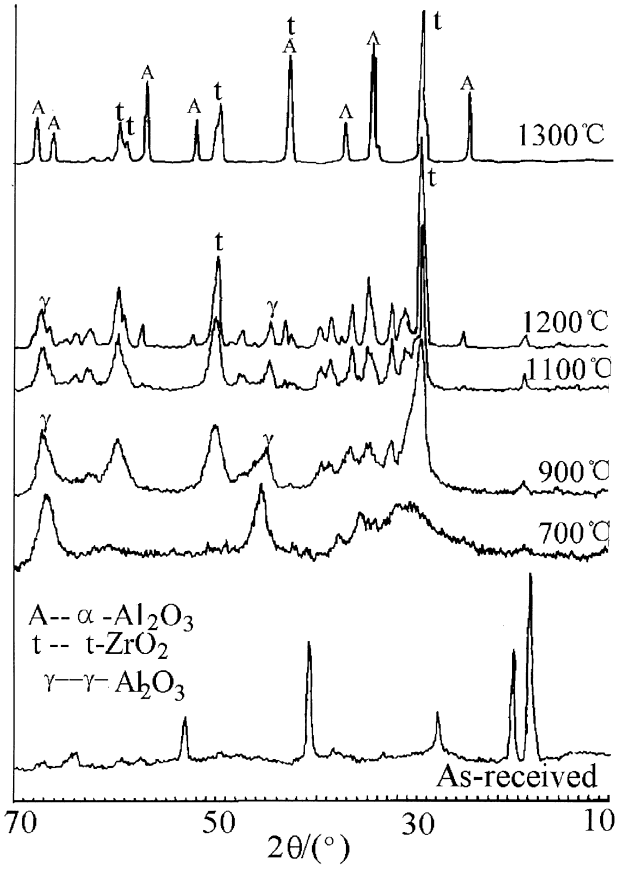

Fig. 2. Phase transformation of Al_2O_3–ZrO_2(3Y)–SiC powder at different temperatures.

3.2 Sintering

The powders were hot pressed at different temperatures, and the relative densities are shown in Fig. 4. It can be seen that the relative density of the sample hot-pressed at 1650°C for 1 h was 99·2%, and 1700°C for 1 h could get to 99·7%. This hot-pressing temperature was similar to that of most Al_2O_3–SiC nanocomposites.[4,5,6] It revealed that it was unnecessary to raise the hot-pressing temperatures of Al_2O_3–SiC nanocomposites for the inclusion of ZrO_2.

3.3 Morphology of surface and fracture cross-section

Figure 5 shows the thermal etched surface of 80 wt% Al_2O_3–15 wt% ZrO_2–5 wt% SiC nanocomposites. Black grains were Al_2O_3, and white particles located among Al_2O_3 grains were ZrO_2. It was observed that the zirconia grains tended to

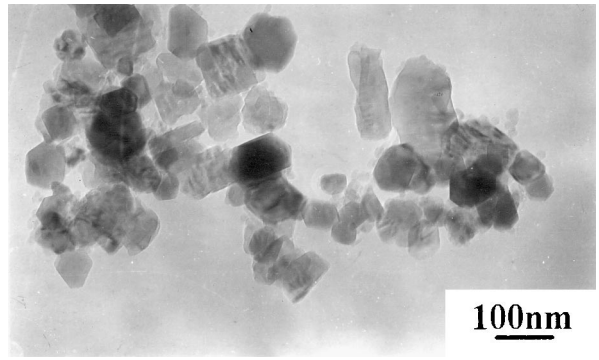

Fig. 3. TEM micrograph of Al_2O_3–ZrO_2(3Y)–SiC composite powder.

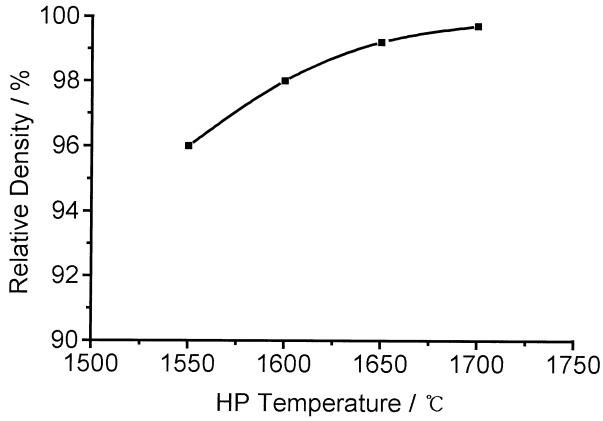

Fig. 4. Relative density vs hot-pressing temperature for the Al_2O_3–ZrO_2(3Y)–SiC composites.

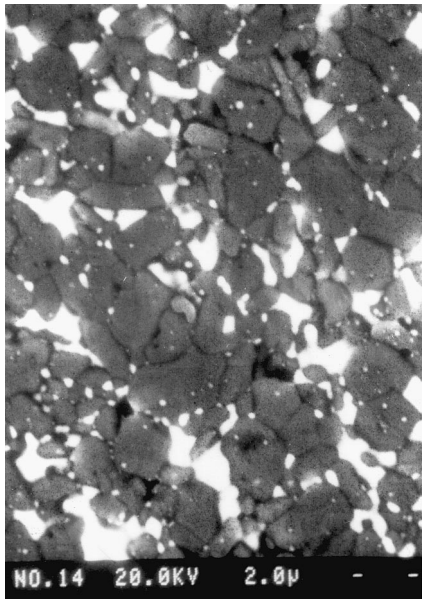

Fig. 5. Thermal etched surface of Al_2O_3–ZrO_2(3Y)–SiC composites.

possess concave boundary segments, whereas the alumina grains tended to be convex with crystallographic facets, which resulted from the lower interfacial energies of ZrO_2/Al_2O_3 than Al_2O_3/Al_2O_3.[15] Nano SiC particles are hardly seen in Fig. 4 for small scale. The size of Al_2O_3 grains calculated by the linear intercept method[16] was 2·1 μm, which was similar to the Al_2O_3 grain size in Al_2O_3–SiC nanocomposites reported by other researchers.[1–6] It revealed that the influence of ZrO_2 inclusion on hindering the grain growth of Al_2O_3–SiC nanocomposites was not significant, which was concident with the consequence of sintering temperature.

Figure 6 was the fracture surface of Al_2O_3–ZrO_2(3Y)–SiC nanocomposites. It can be seen that the fracture mode of Al_2O_3–ZrO_2(3Y)–SiC nanocomposites was transgranular, which was the same as that of Al_2O_3–SiC nanocomposites. There were two different explanations for fracture mode

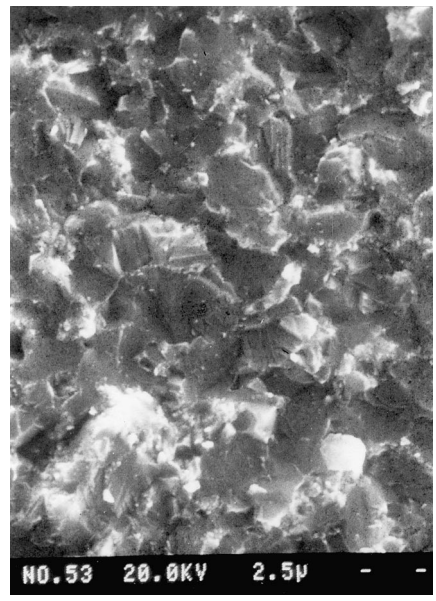

Fig. 6. Fracture surface of Al_2O_3–ZrO_2(3Y)–SiC nanocomposites.

change contrasting to monolithic Al_2O_3, one was that the grains in Al_2O_3–ZrO_2(3Y)–SiC nanocomposites were significantly weakened by addition of SiC and ZrO_2, inducing a crack to propagate into the inside of the grains; the other was that the grain boundaries in nanocomposites were reinforced, inhibiting intergranular crack propagation. However, if the grains of the nanocomposites were weaker than those of the monolith and the strength of the grain boundary was equal between the two materials, it should result in a degraded fracture toughness, for the real area of the crack path in the transgranular fracture mode was small compared to that of the intergranular fracture mode. Hence, the second mechanism was more believable because the fracture toughness of nanocomposites was higher than that of monolith. Figure 6 revealed that the grain boundaries of Al_2O_3–ZrO_2(3Y)–SiC nanocompsites were strengthened although thermal residual stresses in sintered bodies were complex for many phases.

3.4 Microstructure observed by TEM

Figure 7 are TEM micrographs of Al_2O_3–ZrO_2(3Y)–SiC nanocomposites. It can be seen that the shape of most Al_2O_3 grains was elongated in Fig. 7(a) and (c), larger ZrO_2 particles (dark particles) are located among Al_2O_3 grains, and smaller spherical ZrO_2 particles in Al_2O_3 grains just like those shown in Fig. 7(d). Nano SiC particles were well-distributed in Al_2O_3 grains in all micrographs, which indicated that intragranular Al_2O_3–ZrO_2(3Y)–SiC nanocomposites could be obtained using the powder prepared by heterogeneous precipitation. Whether SiC particles were located into ZrO_2 was unclear because the contrast of ZrO_2 was similar to that of SiC in TEM micrograph. But it can be

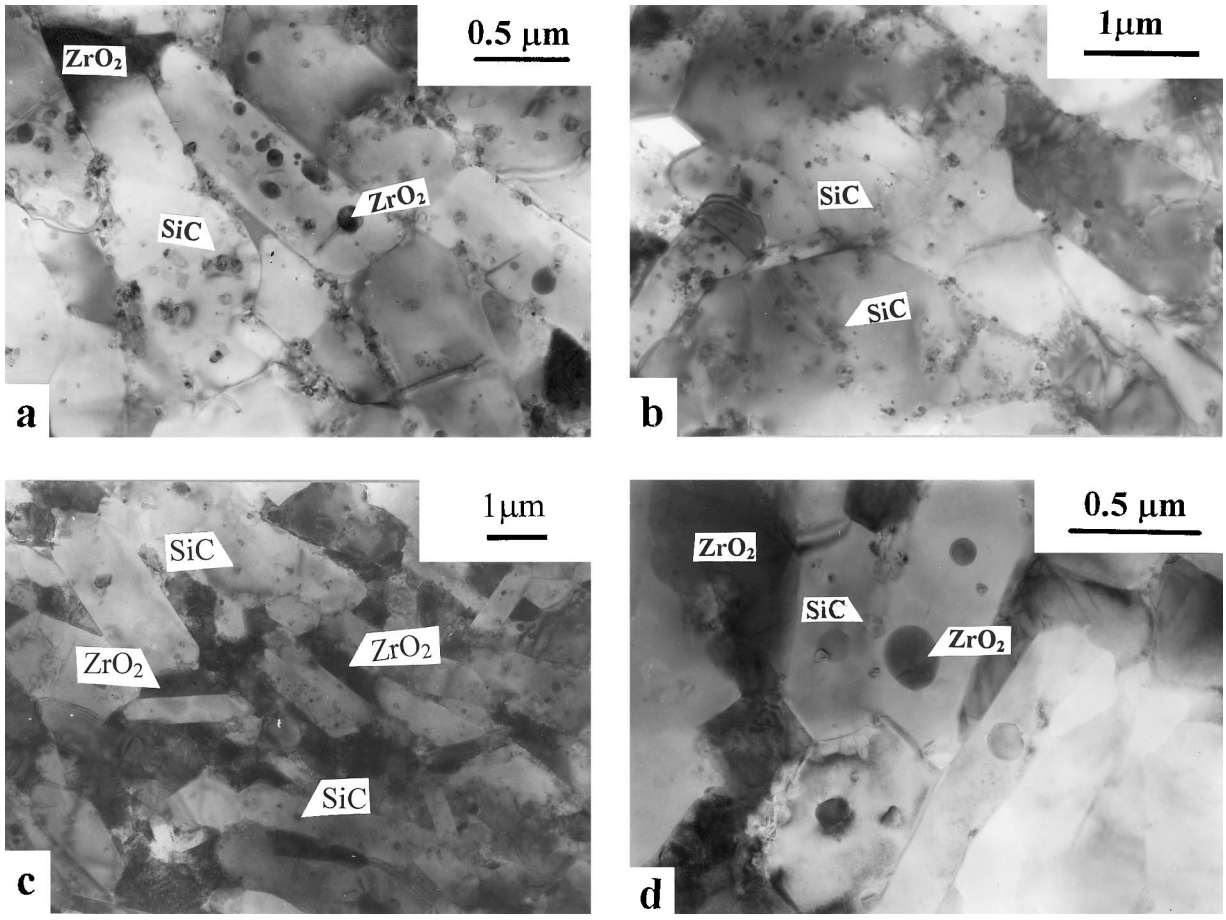

Fig. 7. TEM micrographs of Al_2O_3–ZrO_2(3Y)–SiC nanocomposites.

deduced that SiC particles should be dispersed into Al_2O_3 and ZrO_2 grains equally during the precipitation process. The effect of SiC on the phase transformation of ZrO_2 was interesting because of the thermal residual stress between SiC and ZrO_2. The expansion coefficient of ZrO_2 was larger than that of SiC, and compressive stress would occur on the interface of ZrO_2 and SiC during cooling. The compressive stress would prompt the phase transformation of t-ZrO_2 to m-ZrO_2, and influence the mechanical properties of nanocomposites. If most t-ZrO_2 grain size of nanocomposites were close to critical value of phase transformation, inclusion of SiC would enhance the completion of ZrO_2 phase transformation during cooling from the sintering temperature, and disadvantageous to mechanical properties. Contrarily, if some t-ZrO_2 grain size was too small to transform, inclusion of SiC would promote their phase transformation, and add to the improvement of mechanical properties. Therefore, the influence of SiC inclusion on mechanical properties might be beneficial or deleterious determined by the amount of transformable t-ZrO_2. It revealed that sintering process which affect grain size needed to be controlled carefully to preserve transformable t-ZrO_2 as much as possible, but detail discussion has to be given after more experimental and microstructure observation.

In TEM micrographs, Fig. 7(a) and (c), it can be seen that the shape of most Al_2O_3 grains were elongated in contrast to equiaxed Al_2O_3 grains in Fig. 7(b). Generally, the presence of elongated grain in monolithic Al_2O_3 was believed to be the evidence of the presence of a liquid phase during densification. But in Al_2O_3–SiC nanocomposites, which were prepared with the same raw materials ($AlCl_3$ and SiC) and processing (the heterogeneous precipitation for starting powder), no elongated Al_2O_3 grains had been observed, and little liquid phase could be seen on Al_2O_3/Al_2O_3 and Al_2O_3/SiC interfaces.[17] If the presence of elongated Al_2O_3 grains in Al_2O_3–ZrO_2–SiC nanocomposites was due to impurity liquid phase, many elongated Al_2O_3 grains should also be seen in Al_2O_3-SiC nanocomposites. To investigate the possibility that ZrO_2 forms a number of low temperature eutectics with impurities or Al_2O_3, we observed the Al_2O_3/ZrO_2 interfaces in Al_2O_3–ZrO_2(3Y)–SiC nanocomposites by HRTEM. As shown in Fig. 8, there was no liquid on the Al_2O_3/ZrO_2 interfaces. Therefore, liquid phase resulted in anisotropic grain growth seem difficult to explain this microstructure.

More ZrO_2 particles could be observed around elongated Al_2O_3 grains while fewer ZrO_2 nearby equiaxed Al_2O_3 grains, which may be the reason for forming different Al_2O_3 grain shapes. Most

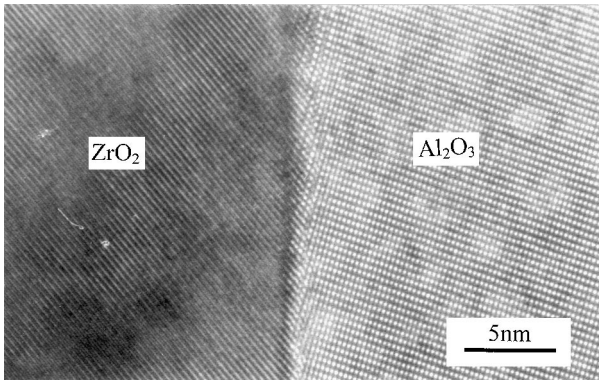

Fig. 8. High resolution TEM micrograph of Al_2O_3/ZrO_2 interfaces.

elongated grains observed through TEM were actually platelike grains just like these shown in Fig. 9.[18] Balmer *et al.*[19] found that platelike Al_2O_3 grains also presented in ZrO_2 toughened Al_2O_3 ceramics (ZTA) during the microstructure development, and took the form of a colony with a common crystallographic orientation. He believed that this morphology was a consequence of the strain energy and diffusional phenomena associated with the $\gamma\alpha$ phase transformation. In Al_2O_3–ZrO_2(3Y)–SiC nanocomposites, the Al_2O_3 grain growth was similar to that in ZTA. Large intrinsic stresses were likely to arise as the growing α-Al_2O_3 ($\rho 3{\cdot}98\ Mg\,m^3$) grains consumed the parent γ-Al_2O_3 phase ($\rho \approx 3{\cdot}65\ Mg\,m^{-3}$) nearby ZrO_2 particles, and Al_2O_3 grains would select anisotropic growth in order to minimize the concomitant strain energy. Contrarily, the γ phase transformation front in monolithic Al_2O_3 moved through a porous, single-phase(γ) parent structure to produce large α-Al_2O_3 without ZrO_2 particles hindering, equiaxed shape inclined to form. Hence, elongated Al_2O_3 grains existed where more ZrO_2 particles can be observed nearby, and equiaxed Al_2O_3 grains grew where no or fewer ZrO_2 particles exist.

3.5 Mechanical properties

Mechanical properties of the 80 wt% Al_2O_3–15 wt% ZrO_2 (3Y)–5 wt% SiC nanocomposites are shown in Table 1.

It can be seen that the strength of sample hot-pressed at 1650°C is lower than that at 1550°C, higher strength may be explained with smaller grain size. Converse to what is expected, the toughness of nanocomposites increases a little comparing to monolithic. Just as discussed above, inclusion of SiC located within ZrO_2 grains would make ZrO_2 phase transformation more easly. If the hot-pressing temperature was high, ZrO_2 grain size was large, some ZrO_2 would transform spontaneously to the m form for compressive stress between intragranular SiC and ZrO_2 during cooling, and the toughening effect of ZrO_2 would disappear.

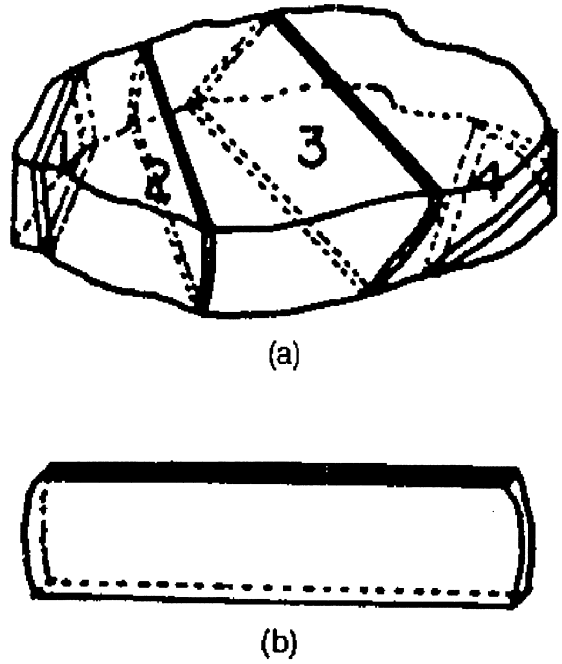

Fig. 9. Indexing procedure for TEM diffraction pattern of flat boundaries of platelike grains: (a) possible thin sections of platelike grains, (b) configuration of most probable section on the TEM image.[18]

Table 1. Mechanical properties of the 80 wt% Al_2O_3–15 wt% ZrO_2 (3Y)–5 wt% SiC nanocomposites.

	Bending strength (MPa)	*Fracture toughness ($MPa\,m^{-1/2}$)*	*Hardness (GPa)*
Sample sintered at 1550°C	555	3·4	16·9
Sample sintered at 1650°C	448	3·8	16·8

Contrarily, the grain size of the sample sintered at lower temperature was smaller, which made ZrO_2 phase transformation difficult, addition of SiC made phase transformation possible and improved the mechanical properties because of the stress-induced transformation of ZrO_2. It indicated that the sintering of Al_2O_3–ZrO_2(3Y)–SiC nanocomposites was important for getting proper ZrO_2 grain size and more transformable t-ZrO_2. We determined m phase content on polished surfaces of nanocomposites by X-ray diffraction, m phase fraction was 54% in samples hot-pressed at 1650°C, and it was 42% in samples hot-pressed at 1550°C. Although m fraction of sample sintered at 1550°C was less than that at 1650°C, for smaller ZrO_2 particle size, both were high. Besides the influence of SiC, the thermal expansion coefficient difference between Al_2O_3 and ZrO_2 also effect the ZrO_2 phase transformation. If Al_2O_3 particles were mainly located within ZrO_2 grains, the influence of Al_2O_3 on ZrO_2 transformation was similar to that of SiC particles because the thermal expansion coefficient

of ZrO_2 was larger than that of Al_2O_3. If most of ZrO_2 particles were intergranular, tensile stresses would occur on the Al_2O_3/ZrO_2 interfaces. Since ZrO_2 transformation leads to a volume increase, these tensile stresses were also advantageous to the ZrO_2 transformation.

To get dense body and high mechanical properties, some new sintering methods were adopted to prepare nanocomposites such as sparking plasma sintering (SPS) which was reported elsewhere.[20] In SPS sintered samples, the strength and toughness of Al_2O_3–ZrO_2(3Y)–SiC nanocomposites were much higher than those of hot-pressed samples, which proved that the powder prepared by the heterogeneous precipitation was successful and the sintering was important to obtain the Al_2O_3–ZrO_2(3Y)–SiC nanocomposites with high mechanical properties.

4 Conclusion

Al_2O_3–ZrO_2(3Y)–SiC composite powders were prepared by the heterogeneous precipation method. The good dispersion of SiC was obtained by ultrasonic vibration and regulating the pH of the SiC aqueous suspension. To get dense sintering body, the selection of calcination temperatures was important, and 1100°C was believed to be the proper temperature. After hot-pressing at 1650°C for 1 h, dense sintering body could be obtained, which indicated that addition of ZrO_2 did not improve the sintering temperature. The fracture mode of Al_2O_3– ZrO_2(3Y)–SiC nanocomposites was transgranular, it proved the boundary strength of nanocomposites was higher than that of monolithic Al_2O_3 which fracture mode was intergranular. Al_2O_3 grain size was about 2 μm, and most SiC particles were located within Al_2O_3 grains. The shape of Al_2O_3 grain was elongated where more ZrO_2 grains were around, and Al_2O_3 was equiaxed where ZrO_2 were less, which resulted from the strain energy and diffusional phenomena associated with the $\gamma \rightarrow \alpha$ phase transformation. SiC particles located within ZrO_2 grains influenced the phase transformation of ZrO_2 and the mechanical properties of nanocomposites. The strength of 80 wt% Al_2O_3–15 wt% ZrO_2–5 wt% SiC nanocomposites was 555 MPa, and toughness was 3·8 MPa $m^{-1/2}$, which were higher than those of monolithic Al_2O_3 ceramics.

References

1. Niihara, K., New design concept of structural ceramics-ceramic nanocomposites. *J. Ceram. Soc. Jpn.*, 1991, **99**, 974–982.
2. Niihara, K., Nakahira, A. and Sekino, T., New nanocomposite structural ceramics. In Nanophase and nanocomposite materials. In *MRS Symposium Proceedings*, Vol. 286, ed. S. Lomarneni, J. C. Parker and G. J. Thomas. Boston, 1992, pp. 405–412.
3. Sternitzke, M., Review: structural ceramic nanocomposites. *J. Eur. Ceram. Soc.*, 1997, **17**, 1061–1082.
4. Stearns, L. C., Zhao, J. and Harmer, M. P. M., Processing and microstructure development in Al_2O_3–SiC nanocomposites. *J. Eur. Ceram. Soc.*, 1992, **100**, 448–453.
5. Zhao, J., Stearns, L. C., Harmer, M. P., Chan, H. M., Miller, G. A. and Cook, R. E., Mechanical behavior of alumina-silicon carbide nanocomposites. *J. Am. Ceram. Soc.*, 1993, **76**, 503–510.
6. Levin, I., Kaplan, W. D., Brandon, D. G. and Layyous, A. A., Effect of SiC submicrometer particle size and content on fracture toughness of alumina-SiC nanocomposites. *J. Am. Ceram. Soc.*, 1995, **78**, 254–256.
7. Shin, D. and Orr, K. K., Microstructure-mechanical property relationships in hot isostatically pressed alumina and zirconia-toughened alumina. *J. Am. Ceram. Soc.*, 1990, **73**, 1181–1188.
8. Witek, S. R. and Butler, E. P., Zirconia particle coarsening and the effects of zirconia additions on the mechanical properties of certain commercial aluminas. *J. Am. Ceram. Soc.*, 1986, **69**, 523–529.
9. Alexander, K. B., Becher, P. F., Wang, X. and Hsuch, C., Internal stresses and the martensite start temperature in alumina-zirconia composites: effects of composition and microstructure. *J. Am. Ceram. Soc.*, 1995, **78**, 291–296.
10. Niihara, K., Morena, R. and Haasselman, D. P. H., Evaluation of K_{1C} of brittle solids by the indentation method with low crack-to-indent ratios. *J. Mater. Sci. Lett.*, 1982, **1**, 13–16.
11. Toraya, H., Yoshimura, M. and Somiya, S., Calibration curve for quantitative analysis of the monoclinic-tetragonal ZrO_2 system by X-ray diffraction. *J. Am. Ceram. Soc.*, 1984, **6**, C–119–C-112.
12. He, Y. J., Winnubst, J. A., Verweij, H. and Burggraaf, A. J., Sinter forging of zirconia toughened alumina. *J. Mater. Sci.*, 1994, **29**, 6505–6512.
13. Exterm, O., Winnubst, L., Leuwerink, T. P. and Burggraaf, A. J., Effect of calcination on the sintering of gel-derived zirconia-toughened alumina. *J. Am. Ceram. Soc.*, 1994, **77**, 2376–2380.
14. Piciacchio, A., Lee, S. and Messing, G. L., Processing and microstructure development in alumina-silicon carbide intragranular particulate composites. *J. Am. Ceram. Soc.*, 1994, **77**, 2157–2164.
15. Wang, J. and Raj, R., Activation energy for the sintering of two-phase alumina/zirconia ceramic. *J. Am. Ceram. Soc.*, 1991, **74**, 1959–1963.
16. Sterns, L. C. and Harmer, M. P., Particle-inhibited grain growth in Al_2O–SiC: I, experimental results, II, equilibrium and kinetic analyses. *J. Am. Ceram. Soc.*, 1996, **79**, 3013–3028.
17. Wang, H. Z., Gao, L., Gui, L. H. and Guo, J. K., Preparation and properties of intergranular Al_2O_3-SiC nanocomposites. *NanoStructured Materials*, 1998, **10**, 947–953.
18. Sing, H. and Coble, R., Morphology of platelike abnormal grains in liquid-phase-sintered alumina. *J. Am. Ceram. Soc.*, 1990, **73**, 2086–2090.
19. Balmer, M. L., Lange, F. F., Jayaram, V. and Levi, C. G., Development of nanocomposite microstructures in ZrO_2–Al_2O_3 via the solution precursor method. *J. Am. Ceram. Soc.*, 1995, **78**, 1489–1494.
20. Gao, L., Wang, H. Z., Hong, J. S., Miyamoto, H., Moyamoto, G., Diaz De la Torre, S. and Nishikawa, Y., Fabrication and mechanical properties of nano-SiC-oxide composites. In *Key Engineering Materials*, Vol. 161–163. Trans Tech Publications. Switzerland, 1999, pp. 401–406.